

CrowdGaussian: Reconstructing High-Fidelity 3D Gaussians for Human Crowd from a Single Image

Yizheng Song¹ Yiyu Zhuang¹ Qipeng Xu¹ Haixiang Wang¹ Jiahe Zhu¹
 Jing Tian¹ Siyu Zhu² Hao Zhu^{1,✉}

¹Nanjing University ²Fudan University.

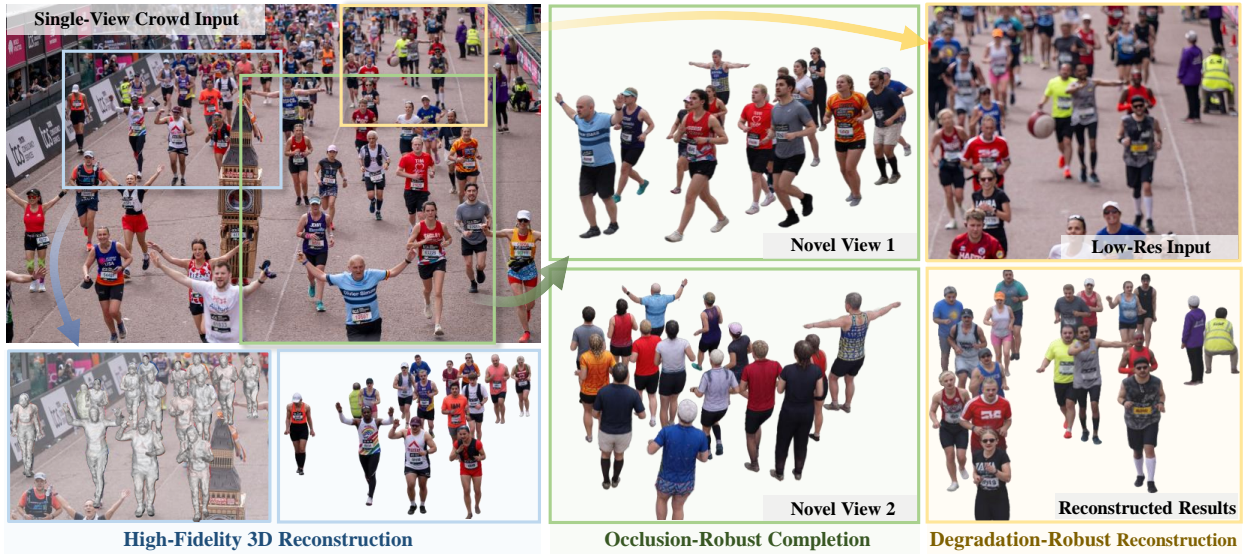


Figure 1. From a single in-the-wild crowd image (**top-left**), CrowdGaussian reconstructs a high-fidelity multi-person 3D Gaussian scene (**blue**). Crucially, our method ensures **occlusion-robust completion**, producing plausible geometry for invisible regions as verified by consistent novel-view rendering (**green**). Furthermore, it demonstrates exceptional **degradation robustness**, successfully recovering sharp details even from low-resolution inputs (**yellow**).

Abstract

Single-view 3D human reconstruction has garnered significant attention in recent years. Despite numerous advancements, prior research has concentrated on reconstructing 3D models from **clear, close-up** images of **individual subjects**, often yielding subpar results in the more prevalent multi-person scenarios. Reconstructing 3D human crowd models is a highly intricate task, laden with challenges such as: 1) extensive occlusions, 2) low clarity, and 3) numerous and various appearances. To address this task, we propose CrowdGaussian, a unified framework that directly reconstructs multi-person 3D Gaussian Splatting (3DGS) representations from single-image inputs. To handle occlusions, we devise a self-supervised adaptation pipeline that enables the pretrained large human model to reconstruct complete 3D humans with plausible geometry

and appearance from heavily occluded inputs. Furthermore, we introduce Self-Calibrated Learning (SCL). This training strategy enables single-step diffusion models to adaptively refine coarse renderings to optimal quality by blending identity-preserving samples with clean/corrupted image pairs. The outputs can be distilled back to enhance the quality of multi-person 3DGS representations. Extensive experiments demonstrate that CrowdGaussian generates photorealistic, geometrically coherent reconstructions of multi-person scenes.

1. Introduction

Creating high-fidelity, animatable 3D human avatars from monocular images is fundamental to advancing immersive applications in virtual reality, teleconferencing, and digi-

tal content creation. Recent breakthroughs in single-image 3D human reconstruction have demonstrated remarkable progress [5, 12, 18, 29, 52, 58]. However, reconstructing the 3D shape and appearance of human crowds from a single image remains an unexplored territory, a scenario that is prevalent but overlooked.

Performing full-body 3D modeling for each individual in a crowd from a single crowd image poses a non-trivial challenge. An intuitive strategy is to integrate human pose estimation algorithms with 3D reconstruction techniques. Specifically, this approach first leverages human pose estimation algorithms to accurately extract crowd pose information, a task well within current capabilities [4, 11, 35–37, 40, 43]. Following this, it crops individual images of each person and leverages single-image human 3D reconstruction algorithms to independently model each person, culminating in the comprehensive 3D reconstruction of the entire crowd.

However, this strategy faces three fundamental challenges. Firstly, in densely populated human crowds, frequent and severe occlusions occur both between individuals and between individuals and objects, often resulting in irregularly absent or obscured body parts. Due to varying person scales and complex occlusion patterns, applying 2D inpainting [19, 22, 55] to recover complete appearances is highly challenging and often produces semantically implausible or geometrically inconsistent completions. Directly feeding such incomplete inputs into existing single-image 3D reconstruction methods yields incomplete geometries with visible transparency artifacts from unobserved regions. Secondly, due to limited 3D supervision and the lack of pose and texture diversity in training datasets, large human models struggle to recover high-frequency details when processing low-resolution person crops, leading to a blurred appearance and a lack of fine details. Lastly, this task places higher demands on efficiency due to the large number of humans to be reconstructed at a single attempt. A unified solution is preferred over concatenating individually trained models for efficient and effective reconstruction.

To address these challenges, we propose CrowdGaussian, a unified two-stage framework for reconstructing the 3D shape and appearance of multiple humans from a single image. In the first stage, we estimate per-person 3D poses and locations using multi-person HMR [40], then segment each individual via SAM [16]. From these (potentially occluded) person crops, we generate an initial coarse multi-person 3DGS [14] representation using LORM (Large Occluded Human Reconstruction Model), which is derived from a pre-trained full body large human model [29] through a self-supervised adaptation framework: by constructing paired data—clean renderings from the frozen teacher and occluded inputs—we distill robust completion capability into the student model without requiring 3D an-

notations. This enables LORM to recover complete geometry and texture even under severe occlusions.

While LORM produces geometrically complete reconstructions, the results may lack high-frequency detail due to low-resolution inputs. Inspired by diffusion-based 3DGS refinement methods [42, 45, 47, 49], we introduce CrowdRefiner, a single-step diffusion model that refines coarse crowd 3DGS representation by leveraging 2D generative priors. We train CrowdRefiner with the Self-Calibrated Learning (SCL) strategy, a novel approach that combines identity-preserving samples with degradation-to-clean pairs. This enables adaptive enhancement—refining under-recovered regions while preserving well-structured areas—without requiring explicit segmentation masks or external labels. The refined outputs serve as pseudo-ground truths for differentiable rendering optimization, resulting in sharper textures and improved local coherence across the multi-person scene.

In summary, our main contributions are:

- We present a robust framework for single-image 3D human reconstruction tailored for **crowd scenes**—a common yet under-explored scenario. Our method achieves significantly superior reconstruction quality compared to state-of-the-art methods, particularly in complex multi-person arrangements.
- We propose a self-supervised fine-tuning strategy that empowers large human reconstruction models to restore complete 3D geometries from occluded inputs, eliminating the need for additional 3D annotations.
- We introduce CrowdRefiner, a single-step diffusion-based refiner trained via Self-Calibrated Learning (SCL). This strategy adaptively enhances 2D renderings from reconstructed 3D Gaussians by balancing refinement strength to prevent over-correction, yielding pseudo-ground truth for 3D quality improvement.

2. Related Work

2.1. Single-Image Human Reconstruction

Early monocular 3D human reconstruction methods primarily relied on parametric models such as SMPL [23, 26] to predict vertex offsets for clothed humans [3, 27, 50], but are constrained by fixed topology and struggle with complex garments or hairstyles. Subsequent works leveraged implicit representation methods [8, 13, 30, 31, 52, 54], enabling arbitrary topologies and providing better flexibility but struggling with complex poses. Recent advances in large reconstruction models (LRMs) [9, 38] have enabled fast, feed-forward 3D human reconstruction from single images [5, 12, 18, 29, 44, 51, 58]. Leveraging transformer architectures and large-scale datasets, these models reduce inductive bias and improve generalization to diverse poses and clothing.

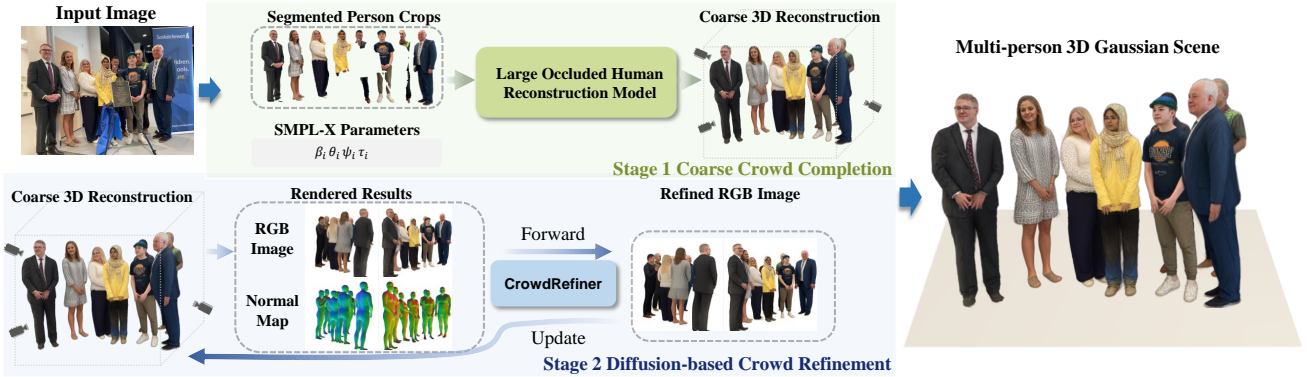


Figure 2. Overview of the proposed CrowdGaussian framework. Our pipeline operates in two stages. In **Stage 1**, we first estimate SMPL-X parameters and segment individuals from the input image. These occluded crops are processed by our **LORM** to hallucinate complete geometries, assembling an initial coarse multi-person 3DGS scene. In **Stage 2**, we render this coarse scene into RGB images and normal maps. Our **CrowdRefiner** leverages these cues to generate high-fidelity pseudo-ground truths, which are then distilled back into the 3D Gaussians via differentiable rendering, significantly enhancing local details and overall sharpness.

However, existing methods often produce incomplete geometric and textural structures when processing irregularly occluded inputs—a common scenario in multi-person scenes. Some approaches attempt to reconstruct 3D humans from incomplete images [6, 39]. Wang *et al.* [39] proposes a coarse-to-fine geometric recovery pipeline followed by progressive texture inpainting to synthesize missing appearances. This multi-stage approach is computationally expensive in a multi-person reconstruction scenario. Moreover, its reliance on limited 3D supervision weakens generalization to diverse poses and clothing. CHROME [6] employs multi-view diffusion to synthesize occlusion-free images under pose control, followed by a 3D reconstruction module that predicts Gaussian representations from the generated views. However, due to subtle misalignments and inconsistencies across the synthesized multi-view images, the resulting 3D scene exhibits texture corruption—particularly around facial regions where fine details are critical.

To address these issues, we introduce **LORM** (Large Occluded Human Reconstruction Model). Adapted from pre-trained large human reconstruction models [29] via a self-supervised framework, LORM enables complete and robust 3D human recovery even from heavily occluded inputs.

2.2. 3D Gaussian Refinement

Very recently, 3D Gaussian Splatting [14] has been widely used for 3D human body representation [29, 51, 56, 58]. Several works explore incorporating geometric priors such as depth to improve the geometric fidelity of 3D Gaussians [17, 57]. Recent approaches further leverage 2D diffusion models as priors to enhance 3D reconstruction quality. Early approaches use diffusion models as iterative optimizers, with denoising steps guiding the update of 3D Gaussians [41, 46, 48], though this incurs a high computational cost due to repeated sampling. To improve efficiency, sev-

eral methods adopt a pseudo-observation paradigm, refining coarse renderings into high-fidelity images for 3D optimization supervision [20, 21, 28, 42, 45, 47, 49].

Deceptive-3DGS [20] refines sparse-view renderings using a diffusion model guided by uncertainty estimates to enhance multi-view consistency. 3DGS-Enhancer [21] trains a video diffusion model on paired low- and high-quality image sequences for temporal coherence in Gaussian Splatting. GenFusion [47] fine-tunes a video diffusion model with masked inpainting to repair view-dependent artifacts in RGB-D sequences. DIFIX [45] employs a single-step diffusion model trained on synthetically corrupted image pairs to correct rendering artifacts. GSFix3D [42] adapts a pretrained diffusion model via task-specific fine-tuning for joint artifact removal and inpainting. GSFIXER [49] introduces a reference-guided video diffusion model that leverages multi-frame cues and geometric features to restore degraded 3DGS renders. Joker [28] uses a 2D diffusion prior to optimize 3D heads with extreme expressions, enabling view-consistent synthesis of features like tongue articulation.

Unlike general-scene methods, we focus on enhancing human crowd 3D Gaussians, where identity preservation and facial details are paramount. We introduce **CrowdRefiner**, a single-step refiner trained via Self-Calibrated Learning to adaptively balance structural preservation and detail enhancement. The resulting high-fidelity pseudo-ground truths are then distilled back into the 3D Gaussians, significantly improving geometric and textural fidelity.

3. Method

3.1. Overview

Given an image $I \in \mathbb{R}^{H \times W \times 3}$ containing N people, our goal is to reconstruct the 3D shape and appearance

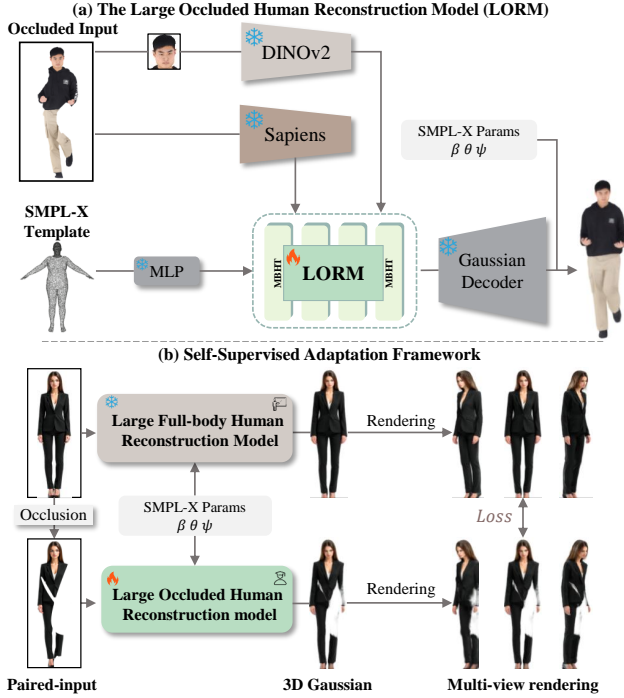


Figure 3. The Large Occluded Human Reconstruction Model (LORM). (a) Architecture. LORM takes an occluded image and a template to reconstruct a complete 3D human. To preserve priors while enabling efficient adaptation, we freeze pre-trained backbones and inject trainable LoRA exclusively into the transformer. (b) Self-Supervised Training. We employ a Teacher-Student framework where the teacher generates clean pseudo-GTs from complete images. These signals guide the student to hallucinate complete geometries from occluded inputs via self-distillation, achieving robustness without external 3D supervision.

of all individuals into coherent 3D Gaussian Splatting (3DGS) representations. As illustrated in Figure 2, we propose CrowdGaussian, a unified framework for single-image multi-person 3D reconstruction.

Our pipeline proceeds in two main stages: *Coarse Crowd Completion* and *Diffusion-based Crowd Refinement*.

In *Coarse Crowd Completion*, we estimate per-person 3D poses and camera-space positions using a multi-person HMR model [40]. Guided by these estimates, we segment each individual from the background using SAM [16], yielding N person crops that are often incomplete due to occlusions. We then generate an initial coarse multi-person 3DGS scene by applying the Large Occluded Human Reconstruction Model (LORM) to each segmented crop—enabling complete geometry recovery despite missing regions. This stage is detailed in Section 3.2.

In *Diffusion-based Crowd Refinement*, we enhance the reconstructed multi-person 3D Gaussians using a single-step diffusion model. To prevent over-refinement, we train it with a Self-Calibrated Learning (SCL) strategy that adap-

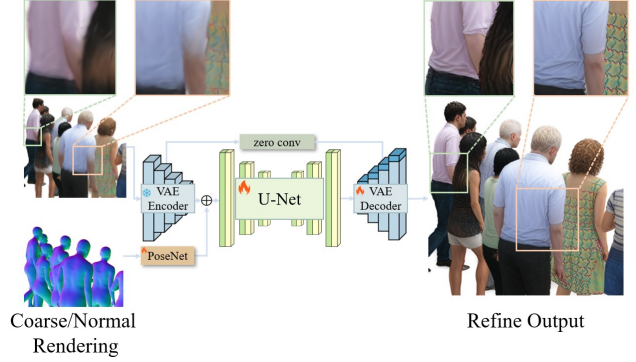


Figure 4. Architecture of CrowdRefiner, our single-step diffusion refiner for Crowd 3D Gaussians enhancement. Given a coarse rendering and its corresponding SMPL normal map as geometric prior, CrowdRefiner generates a high-fidelity refined output. The model is fine-tuned from SD-Turbo with a LoRA-finetuned VAE decoder and a trainable PoseNet, while the VAE encoder remains frozen. Zoom-in regions highlight significant improvements in local details such as hair and clothing textures.

tively preserves well-recovered regions while enhancing under-refined details. The refined outputs serve as high-fidelity pseudo-ground truths, which are distilled back into the 3D Gaussians via differentiable rendering to improve both local detail and global coherence. This refinement pipeline is described in Section 3.3.

3.2. Occlusion-free 3D Human Reconstruction

Preliminaries. We build upon a pre-trained large human reconstruction model [29] as our foundation, which takes a complete human image as input and outputs a 3D human represented as a set of 3D Gaussian:

$$\mathcal{G} = \{(\boldsymbol{\mu}_i, \boldsymbol{\Sigma}_i, \alpha_i, \mathbf{c}_i)\}_{i=1}^N, \quad (1)$$

where $\boldsymbol{\mu}_i \in \mathbb{R}^3$ is the center, $\boldsymbol{\Sigma}_i \in \mathbb{R}^{3 \times 3}$ the covariance, $\alpha_i \in [0, 1]$ the opacity, and $\mathbf{c}_i \in \mathbb{R}^3$ the view-dependent color. The model employs a Multimodal Body-Head Transformer (MBHT) to fuse SMPL-based geometric priors with visual features extracted by the *frozen* Sapiens encoder.

Though the Sapiens encoder—being a Masked Autoencoder (MAE) [7]—possesses inherent potential for handling partial visibility, the human reconstruction model lacks occlusion-aware training. Consequently, it fails to produce coherent geometries when processing occluded inputs, as its transformer backbone struggles to integrate incomplete visual features. To address this limitation, we propose LORM, a Large Occluded Human Reconstruction Model, which is obtained by applying our parameter-efficient self-supervised adaptation framework to the pre-trained model.

Occlusion-free 3D Human Reconstruction. We propose the Large Occluded Human Reconstruction Model (LORM) to recover complete 3D geometries from occluded single-view inputs (I_{occ}), as shown in Figure 3 (a). To leverage robust 2D-to-3D generative priors, we initialize LORM with



Figure 5. Effect of Self-Calibrated Learning (SCL). Without SCL (middle), the model tends to over-refine, causing facial distortions and artifacts. With SCL (right), structural integrity is preserved while details are enhanced, demonstrating adaptive refinement enabled by mixed identity supervision during training.

a pre-trained large reconstruction model [29]. However, this baseline fails on occlusions due to domain gaps. Fine-tuning with external 3D supervision is suboptimal, as it often amplifies geometric bias inherent in monocular ambiguity, damaging pre-trained priors. To circumvent this, we introduce a self-supervised teacher-student framework that adapts the model using only single-view images, ensuring geometric consistency without external 3D annotations.

Self-Supervised Adaptation Framework. The training framework is illustrated in Figure 3 (b). We construct training pairs from thousands of frontal images from the HuGe100K dataset [58]. In the teacher stream, the *frozen* pre-trained model processes a complete image I_{full} to yield a complete 3D Gaussian representation $\mathcal{G}_{\text{full}}$. We render $\mathcal{G}_{\text{full}}$ from V novel viewpoints to generate clean pseudo-ground truths:

$$R_{\text{clean}}^{(v)} = \text{Render}(\mathcal{G}_{\text{full}}, \theta_v), \quad v = 1, \dots, V, \quad (2)$$

where θ_v denotes the camera pose for the v -th view.

In the student stream, to simulate realistic occlusions, we generate I_{occ} by applying irregular masks—combining random Bézier curve-based erasures and keypoint-centered ellipses—to I_{full} . The student model (LORM) predicts 3D Gaussians from I_{occ} , which are rendered into coarse views:

$$R_{\text{coarse}}^{(v)} = \text{Render}(\text{LORM}(I_{\text{occ}}, \theta), \theta_v). \quad (3)$$

We optimize the adapted parameters using a self-distillation loss that aligns the coarse student outputs with the clean teacher renderings:

$$\mathcal{L}_{\text{self-distill}} = \sum_{v=1}^V \left(\lambda_{\text{rgb}} \|R_{\text{clean}}^{(v)} - R_{\text{coarse}}^{(v)}\|_2 + \lambda_{\text{ssim}} \left(1 - \text{SSIM}(R_{\text{clean}}^{(v)}, R_{\text{coarse}}^{(v)}) \right) \right), \quad (4)$$

where λ_{rgb} and λ_{ssim} are balancing weights.

To minimize disruption to pre-trained visual priors while maintaining efficiency, we inject trainable Low-Rank Adaptation (LoRA) modules [10] exclusively into the MBHT transformer. The Sapiens encoder and Gaussian decoder remain frozen. This design preserves robust feature extraction while focusing adaptation solely on hallucinating complete 3D structures from incomplete features.

3.3. Multi-Person Scene Refinement

Although LORM recovers complete geometries, the initial crowd 3DGS representation often suffers from over-smoothing and lacks high-frequency details due to the resolution limits of the reconstruction model. To address this, we introduce CrowdRefiner, a single-step diffusion model specifically trained to act as a high-fidelity detail enhancer. Unlike standard diffusion models, CrowdRefiner is trained to learn a geometry-aware refinement policy and is applied *online* to distill details back into the crowd 3DGS via an iterative optimization pipeline.

CrowdRefiner Design and Training. Built upon SD-Turbo [25, 32, 45], CrowdRefiner is designed for efficient single-step inference, as shown in Figure 4. To ensure geometric consistency, the model is additionally conditioned on its corresponding SMPL normal map N to the coarse RGB rendering R_{coarse} . Specifically, we encode the normal map via a lightweight pose encoder and the RGB image through the VAE encoder. These multi-modal features are then injected into the UNet backbone to guide the generation process. To preserve fine-grained image details during refinement, we fine-tune it using LoRA adapters injected into the decoder, while keeping the VAE encoder frozen.

Training is performed on a synthetic dataset constructed from THuman2.1 [53], comprising pairs of LORM-generated coarse renderings and high-quality ground truths. However, we observe that standard supervised training on these degradation-to-clean pairs often leads to **over-refinement**, resulting in facial distortions and artifacts (as shown in Figure 5).

To mitigate this, we introduce the **Self-Calibrated Learning (SCL) strategy**. This approach fosters a *balanced refinement* policy by randomly mixing standard degradation pairs $(R_{\text{coarse}}, R_{\text{gt}})$ with identity-preserving samples $(R_{\text{gt}}, R_{\text{gt}})$ during training. This mixed supervision scheme encourages the model to *selectively* enhance under-recovered regions while strictly preserving well-structured areas.

The model is trained with a composite loss:

$$\mathcal{L}_{\text{diff}} = \lambda_{L2} \mathcal{L}_{L2} + \lambda_{\text{lpiPs}} \mathcal{L}_{\text{LPIPS}} + \lambda_{\text{ssim}} \mathcal{L}_{\text{SSIM}} + \lambda_{\text{gram}} \mathcal{L}_{\text{Gram}}, \quad (5)$$

where the L2, LPIPS, and SSIM losses ensure pixel-level accuracy and perceptual similarity. A Gram loss [45] is ad-

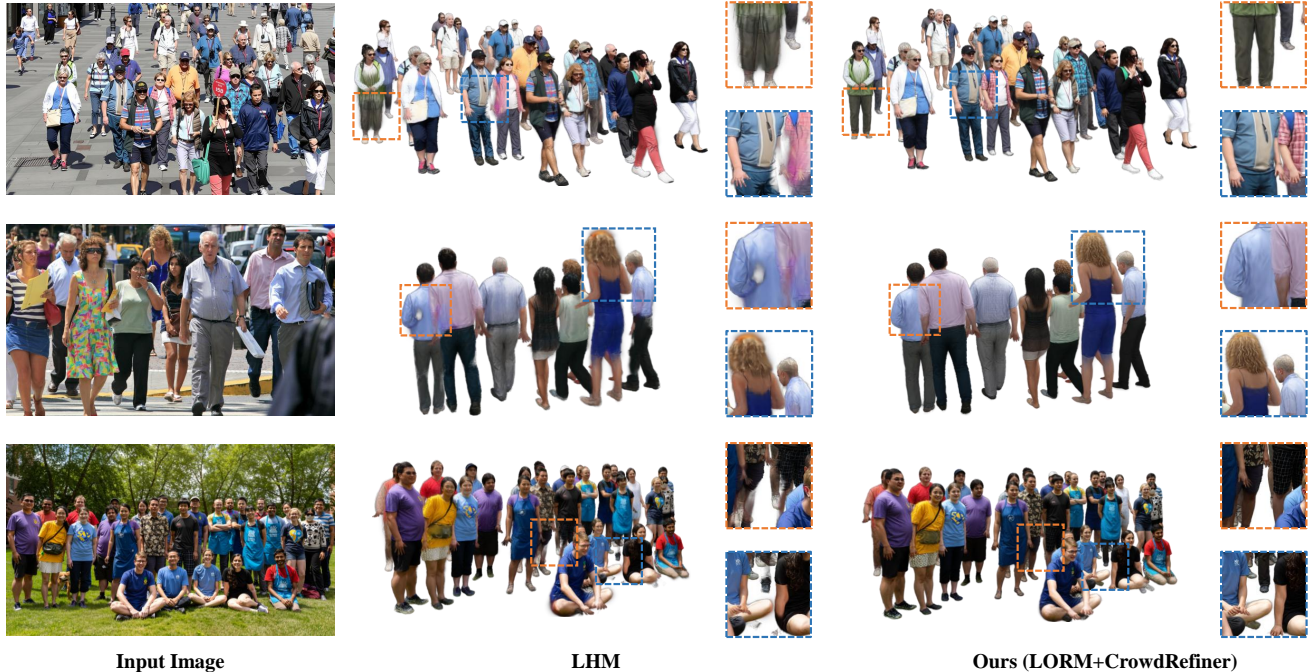


Figure 6. Single-shot multi-person 3D reconstruction. While the LHM baseline (**middle**) struggles with artifacts and missing details in occluded regions, our method (**right**) generates complete geometry and high-fidelity textures. Zoom-ins highlight our superior recovery of faces and hands, validating robustness to occlusion and low-resolution inputs.

ditionally applied to enforce texture sharpness by matching high-order feature statistics.

Crowd 3D Gaussians Refinement. During the inference stage, we apply the pre-trained CrowdRefiner to enhance the target crowd scene. To avoid the prohibitive computational costs associated with processing individuals sequentially, we adopt a holistic strategy to refine local crowd segments simultaneously.

Specifically, to handle complex spatial arrangements, we first group individuals into spatially coherent clusters using DBSCAN [33] based on their root positions. For each cluster, we render coarse views $R_{\text{coarse}}^{(v)}$ and process them through CrowdRefiner to generate high-fidelity pseudo-ground truths $R_{\text{refined}}^{(v)}$.

Finally, we distill these refined priors back into the 3D Gaussians by iteratively minimizing the difference between the current rendering and the refined target:

$$\mathcal{L}_{\text{optim}} = \|R_{\text{refined}}^{(v)} - R_{\text{coarse}}^{(v)}\|_1 + \lambda_{\text{ssim}}(1 - \text{SSIM}(R_{\text{refined}}^{(v)}, R_{\text{coarse}}^{(v)})). \quad (6)$$

This distillation process effectively transfers the generative details into the 3D representation, significantly improving geometric sharpness and local fidelity across the crowd.

4. Experiments

4.1. Implementation Details

Data Construction for LORM Training. We select 1,002 frontal images from HuGe100K [58] for the training of LORM. We initialize our model using the pre-trained weights from LHM-500M-HF. During end-to-end optimization, LORM renders its 3DGS representation from 24 fixed camera viewpoints using differentiable rendering.

Data Construction for CrowdRefiner Training. For the training of CrowdRefiner, we utilize a paired dataset constructed with identities from THuman2.1 [53]. We built 114 synthetic multi-person scenes by composing the high-quality meshes in diverse spatial configurations. For each scene, we generate paired renderings from 126 viewpoints on a hemisphere: (1) the high-fidelity ground-truth R_{gt} is rendered from the original THuman meshes, (2) the corresponding coarse input R_{coarse} is rendered from the 3DGS representation reconstructed by our Stage 1 LORM. This process yields our final $(R_{\text{coarse}}, R_{\text{gt}})$ training pairs, (3) the normal map from SMPL-X model. Of these 114 scenes, 91 (80%) are used for training and 23 for testing.

4.2. Comparisons

Multi-Person Reconstruction. Figure 6 presents qualitative results on challenging in-the-wild crowd scenes. Despite severe inter-person and object occlusions, as well as the low resolution of individual person crops, our



Figure 7. Qualitative comparison on occluded in-the-wild images. Mesh-based methods (PSHuman, SyncHuman) fail to recover complete geometry. 3DGS-based approaches (IDOL, LHM) produce transparency artifacts or incoherent and distorted textures in missing regions. In contrast, our method reconstructs complete 3D geometry and texture, demonstrating robustness to real-world occlusion.

Table 1. Quantitative comparison on occluded human reconstruction (THuman2.1) with randomly applied masks.

Method	PSNR \uparrow	SSIM \uparrow	LPIPS \downarrow
IDOL [58]	18.063	0.919	0.994
LHM [29]	18.171	0.918	1.012
LORM	18.566	0.923	0.956
LORM+CrowdRefiner	18.619	0.931	0.914

framework successfully reconstructs high-fidelity multi-person 3DGS representations. Compared to the baseline LHM—where missing regions often result in transparency artifacts and blurred details (e.g., facial features, hands)—our full pipeline leverages LORM for robust structural completion and CrowdRefiner for texture refinement. This synergy produces complete geometry with sharp, coherent appearance. Zoom-in views highlight significant improvements in fine-scale details, demonstrating the effectiveness of our approach in recovering both shape and appearance under real-world conditions.

Occlusion-Robust Human Reconstruction. We benchmark against SOTA methods (LHM [29], PSHuman [18], SyncHuman [5], IDOL [58]) on naturally occluded in-the-wild images in Figure 7.

Lacking specific design for occlusions, these baselines often yield incomplete geometries plagued by visible transparency artifacts. In contrast, LORM recovers complete

Table 2. Quantitative comparison under increasing occlusion ratios (20%–60%) on THuman2.1.

Method	Occlusion Ratio	PSNR \uparrow	SSIM \uparrow	LPIPS \downarrow
IDOL	20%	18.196	0.921	0.978
	40%	17.412	0.914	1.027
	60%	16.667	0.909	1.063
LHM	20%	17.945	0.919	1.006
	40%	17.709	0.916	1.026
	60%	17.551	0.915	1.037
LORM	20%	18.428	0.923	0.947
	40%	18.199	0.921	0.965
	60%	18.116	0.919	0.972

and structurally sound shapes, while the 3D refinement with CrowdRefiner further enhances local fidelity and texture sharpness. This confirms our pipeline’s ability to ensure complete geometry and sharp textures despite severe input incompleteness.

Quantitatively, we first simulate irregular occlusions using random masks, as reported in Table 1. Our full pipeline achieves the best PSNR, SSIM, and LPIPS, outperforming all baselines.

Second, we assess robustness under increasing occlusion ratios (20%–60%) in Table 2. While LHM and IDOL suffer severe degradation as occlusion increases, LORM maintains stable performance, confirming its strong resilience.

Degradation-Robust Human Reconstruction. To evalu-

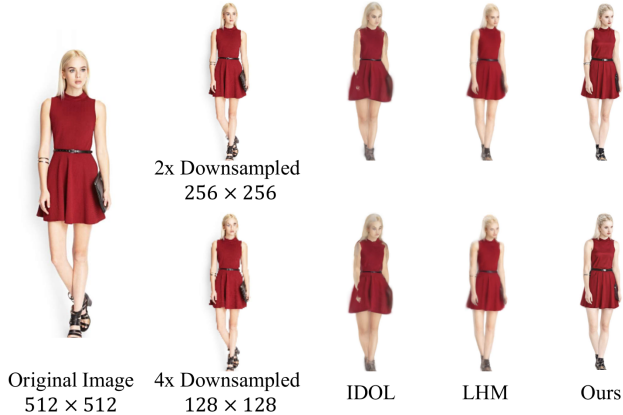


Figure 8. Robustness to resolution degradation. The leftmost column shows the original image, followed by inputs downsampled by 2 \times and 4 \times . Subsequent columns compare reconstructions from IDOL, LHM, and Ours. Even from significantly downsampled inputs, our approach consistently recovers high-fidelity geometry and sharp textures, demonstrating superior robustness to input resolution degradation compared to baselines.

Table 3. Ablation study on the SCL strategy and geometric conditioning inputs for the refiner. Results demonstrate that both SCL and the additional normal map input contribute to consistent improvements in generation quality, providing higher-fidelity supervision for the subsequent stage.

SCL	Normal	PSNR \uparrow	SSIM \uparrow	LPIPS \downarrow
—	—	20.013	0.888	0.141
—	✓	20.130	0.892	0.138
✓	—	20.382	0.896	0.129
✓	✓	20.790	0.901	0.122

ate robustness against resolution degradation, we downsample the original image by 2 \times and 4 \times and reconstruct each using IDOL, LHM, and our full pipeline.

As shown in Figure 8, baselines suffer significantly from the resolution drop, exhibiting over-smoothed textures and boundary artifacts. In contrast, our method leverages generative priors to recover sharper textures and coherent structures. This demonstrates that our framework effectively mitigates input degradation, enabling high-fidelity reconstruction even from severely low-resolution inputs.

4.3. Ablation Study

We evaluate on a held-out set of 23 synthetic multi-person scenes from THuman2.1, totaling 2,622 pairs of LORM and GT mesh renderings.

Effect of SCL Strategy. We evaluate the effectiveness of Self-Calibrated Learning (SCL) on the 23 test scenes. As shown in Figure 5, without SCL, the refiner suffers from over-refinement, producing facial distortions and texture artifacts due to aggressive enhancement. In contrast,

with SCL enabled, the model adaptively preserves well-recovered regions while refining incomplete areas, maintaining structural integrity.

This improvement is further validated by the quantitative results in Table 3, where metrics evaluate the quality of the refined 2D outputs by CrowdRefiner. As shown, disabling SCL results in a noticeable performance decline across both the RGB-only and RGB+Normal configurations. This confirms that SCL plays a critical role in balancing refinement strength and preventing hallucinations, ensuring the generation of high-fidelity pseudo-ground truths for the subsequent 3D distillation process.

Ablation on Geometric Conditioning. We assess the importance of SMPL normal maps as 3D geometric priors. By training a variant without normal map conditioning (RGB only), we observe a clear performance drop in the refined outputs, as shown in Table 3. This degradation, particularly in PSNR and LPIPS, confirms that explicit geometric cues are essential to prevent structural ambiguity, thereby improving pose consistency and texture alignment.

5. Conclusion

In this work, we present CrowdGaussian, a framework for single-image multi-person 3D human reconstruction. Our approach addresses occlusion and low-resolution challenges through two key components. First, LORM (Large Occluded Human Reconstruction Model) enables complete 3D geometry recovery from heavily occluded inputs via self-supervised adaptation, without requiring 3D annotations. Second, CrowdRefiner—a diffusion-based refiner trained with Self-Calibrated Learning (SCL)—generates high-fidelity pseudo-ground truths from coarse renderings and distills them back into the 3DGS via differentiable rendering, enhancing both local detail and global coherence.

6. Limitations

First, we rely on off-the-shelf estimators for pose, spatial location, and body shape; consequently, severe initialization errors may propagate to the final geometry, making hand reconstruction challenging as our pipeline is not designed to correct fundamental structural misalignments. Second, while our method recovers plausible details for occluded regions or degraded inputs, severely low resolution may lead to inconsistent identities, and these hallucinated details may not always be factually faithful to the unobserved ground truth (e.g., specific logos).

Acknowledgements

This work was supported in part by the National Natural Science Foundation of China under Grant U25B2046.

References

- [1] <https://huggingface.co/alimama-creative/FLUX.1-dev-Controlnet-Inpainting-Beta>. 2
- [2] Google Images. <https://images.google.com/>. 4
- [3] Thimeo Alldieck, Marcus Magnor, Weipeng Xu, Christian Theobalt, and Gerard Pons-Moll. Detailed human avatars from monocular video. In *2018 International Conference on 3D Vision (3DV)*, pages 98–109. IEEE, 2018. 2
- [4] Fabien Baradel, Matthieu Armando, Salma Galaoui, Romain Brégier, Philippe Weinzaepfel, Grégory Rogez, and Thomas Lucas. Multi-hmr: Multi-person whole-body human mesh recovery in a single shot. In *European Conference on Computer Vision*, pages 202–218. Springer, 2024. 2
- [5] Wenye Chen, Peng Li, Wangguandong Zheng, Chengfeng Zhao, Mengfei Li, Yaolong Zhu, Zhiyang Dou, Ronggang Wang, and Yuan Liu. Synchuman: Synchronizing 2d and 3d generative models for single-view human reconstruction. *arXiv preprint arXiv:2510.07723*, 2025. 2, 7
- [6] Arindam Dutta, Meng Zheng, Zhongpai Gao, Benjamin Planche, Anwesa Choudhuri, Terrence Chen, Amit K Roy-Chowdhury, and Ziyang Wu. Chrome: Clothed human reconstruction with occlusion-resilience and multiview-consistency from a single image. In *Proceedings of the IEEE/CVF International Conference on Computer Vision*, pages 9124–9135, 2025. 3
- [7] Kaiming He, Xinlei Chen, Saining Xie, Yanghao Li, Piotr Dollár, and Ross Girshick. Masked autoencoders are scalable vision learners. In *Proceedings of the IEEE/CVF Conference on Computer Vision and Pattern Recognition*, pages 16000–16009, 2022. 4
- [8] Tong He, Yuanlu Xu, Shunsuke Saito, Stefano Soatto, and Tony Tung. Arch++: Animation-ready clothed human reconstruction revisited. In *Proceedings of the IEEE/CVF International Conference on Computer Vision*, pages 11046–11056, 2021. 2
- [9] Yicong Hong, Kai Zhang, Jiuxiang Gu, Sai Bi, Yang Zhou, Difan Liu, Feng Liu, Kalyan Sunkavalli, Trung Bui, and Hao Tan. Lrm: Large reconstruction model for single image to 3d. *arXiv preprint arXiv:2311.04400*, 2023. 2
- [10] Edward J Hu, Yelong Shen, Phillip Wallis, Zeyuan Allen-Zhu, Yuanzhi Li, Shean Wang, Lu Wang, Weizhu Chen, et al. Lora: Low-rank adaptation of large language models. *ICLR*, 1(2):3, 2022. 5
- [11] Jing Huang, Hao Wen, Tianyi Zhou, Haozhe Lin, Yu-Kun Lai, and Kun Li. Rcr: Robust crowd reconstruction with up-right space from a single large-scene image. *arXiv preprint arXiv:2411.06232*, 2024. 2
- [12] Yangyi Huang, Ye Yuan, Xueting Li, Jan Kautz, and Umar Iqbal. Adahuman: Animatable detailed 3d human generation with compositional multiview diffusion. In *Proceedings of the IEEE/CVF International Conference on Computer Vision*, pages 13533–13543, 2025. 2
- [13] Zeng Huang, Yuanlu Xu, Christoph Lassner, Hao Li, and Tony Tung. Arch: Animatable reconstruction of clothed humans. In *Proceedings of the IEEE/CVF Conference on Computer Vision and Pattern Recognition*, pages 3093–3102, 2020. 2
- [14] Bernhard Kerbl, Georgios Kopanas, Thomas Leimkühler, and George Drettakis. 3d gaussian splatting for real-time radiance field rendering. *ACM Trans. Graph.*, 42(4):139–1, 2023. 2, 3
- [15] Diederik P Kingma and Jimmy Ba. Adam: A method for stochastic optimization. *arXiv preprint arXiv:1412.6980*, 2014. 2, 4
- [16] Alexander Kirillov, Eric Mintun, Nikhila Ravi, Hanzi Mao, Chloe Rolland, Laura Gustafson, Tete Xiao, Spencer Whitehead, Alexander C Berg, Wan-Yen Lo, et al. Segment anything. In *Proceedings of the IEEE/CVF International Conference on Computer Vision*, pages 4015–4026, 2023. 2, 4
- [17] Raja Kumar and Vanshika Vats. Few-shot novel view synthesis using depth aware 3d gaussian splatting. In *European Conference on Computer Vision*, pages 1–13. Springer, 2024. 3
- [18] Peng Li, Wangguandong Zheng, Yuan Liu, Tao Yu, Yangguang Li, Xingqun Qi, Xiaowei Chi, Siyu Xia, Yan-Pei Cao, Wei Xue, et al. Pshuman: Photorealistic single-image 3d human reconstruction using cross-scale multiview diffusion and explicit remeshing. In *Proceedings of the Computer Vision and Pattern Recognition Conference*, pages 16008–16018, 2025. 2, 7
- [19] Guoqiang Liang, Jiahao Hu, Qingyue Wang, and Shizhou Zhang. Dmat: A dynamic mask-aware transformer for human de-occlusion. *arXiv preprint arXiv:2402.04558*, 2024. 2
- [20] Xinhang Liu, Jiaben Chen, Shiu-Hong Kao, Yu-Wing Tai, and Chi-Keung Tang. Deceptive-nerf/3dgs: Diffusion-generated pseudo-observations for high-quality sparse-view reconstruction. In *European Conference on Computer Vision*, pages 337–355. Springer, 2024. 3
- [21] Xi Liu, Chaoyi Zhou, and Siyu Huang. 3dgs-enhancer: Enhancing unbounded 3d gaussian splatting with view-consistent 2d diffusion priors. *Advances in Neural Information Processing Systems*, 37:133305–133327, 2024. 3
- [22] Zhengzhe Liu, Qing Liu, Chirui Chang, Jianming Zhang, Daniil Pakhomov, Haitian Zheng, Zhe Lin, Daniel Cohen-Or, and Chi-Wing Fu. Object-level scene deocclusion. In *ACM SIGGRAPH 2024 Conference Papers*, pages 1–11, 2024. 2
- [23] Matthew Loper, Naureen Mahmood, Javier Romero, Gerard Pons-Moll, and Michael J Black. Smpl: A skinned multi-person linear model. In *Seminal Graphics Papers: Pushing the Boundaries, Volume 2*, pages 851–866. 2023. 2
- [24] Camillo Lugaresi, Jiuqiang Tang, Hadon Nash, Chris McClanahan, Esha Uboweja, Michael Hays, Fan Zhang, Chuo-Ling Chang, Ming Guang Yong, Juhyun Lee, et al. Mediapipe: A framework for building perception pipelines. *arXiv preprint arXiv:1906.08172*, 2019. 1
- [25] Gaurav Parmar, Taesung Park, Srinivasa Narasimhan, and Jun-Yan Zhu. One-step image translation with text-to-image models. *arXiv preprint arXiv:2403.12036*, 2024. 5
- [26] Georgios Pavlakos, Vasileios Choutas, Nima Ghorbani, Timo Bolkart, Ahmed AA Osman, Dimitrios Tzionas, and Michael J Black. Expressive body capture: 3d hands, face, and body from a single image. In *Proceedings of the IEEE/CVF Conference on Computer Vision and Pattern Recognition*, pages 10975–10985, 2019. 2

- [27] Georgios Pavlakos, Nikos Kolotouros, and Kostas Daniilidis. Texturepose: Supervising human mesh estimation with texture consistency. In *Proceedings of the IEEE/CVF International Conference on Computer Vision*, pages 803–812, 2019. 2
- [28] Malte Prinzler, Egor Zakharov, Vanessa Sklyarova, Berna Kabadayi, and Justus Thies. Joker: Conditional 3d head synthesis with extreme facial expressions. In *2025 International Conference on 3D Vision (3DV)*, pages 1583–1593. IEEE, 2025. 3
- [29] Lingteng Qiu, Xiaodong Gu, Peihao Li, Qi Zuo, Weichao Shen, Junfei Zhang, Kejie Qiu, Weihao Yuan, Guanying Chen, Zilong Dong, et al. Lhm: Large animatable human reconstruction model for single image to 3d in seconds. In *Proceedings of the IEEE/CVF International Conference on Computer Vision*, pages 14184–14194, 2025. 2, 3, 4, 5, 7
- [30] Shunsuke Saito, Zeng Huang, Ryota Natsume, Shigeo Morishima, Angjoo Kanazawa, and Hao Li. Pifu: Pixel-aligned implicit function for high-resolution clothed human digitization. In *Proceedings of the IEEE/CVF International Conference on Computer Vision*, pages 2304–2314, 2019. 2
- [31] Shunsuke Saito, Tomas Simon, Jason Saragih, and Hanbyul Joo. Pifuhd: Multi-level pixel-aligned implicit function for high-resolution 3d human digitization. In *Proceedings of the IEEE/CVF Conference on Computer Vision and Pattern Recognition*, pages 84–93, 2020. 2
- [32] Axel Sauer, Dominik Lorenz, Andreas Blattmann, and Robin Rombach. Adversarial diffusion distillation. In *European Conference on Computer Vision*, pages 87–103. Springer, 2024. 5, 2
- [33] Erich Schubert, Jörg Sander, Martin Ester, Hans Peter Kriegel, and Xiaowei Xu. DbSCAN revisited, revisited: why and how you should (still) use dbSCAN. *ACM Transactions on Database Systems (TODS)*, 42(3):1–21, 2017. 6
- [34] Karen Simonyan and Andrew Zisserman. Very deep convolutional networks for large-scale image recognition. *arXiv preprint arXiv:1409.1556*, 2014. 4
- [35] Qingping Sun, Yanjun Wang, Ailing Zeng, Wanqi Yin, Chen Wei, Wenjia Wang, Haiyi Mei, Chi-Sing Leung, Ziwei Liu, Lei Yang, et al. Aios: All-in-one-stage expressive human pose and shape estimation. In *Proceedings of the IEEE/CVF Conference on Computer Vision and Pattern Recognition*, pages 1834–1843, 2024. 2
- [36] Yu Sun, Wu Liu, Qian Bao, Yili Fu, Tao Mei, and Michael J Black. Putting people in their place: Monocular regression of 3d people in depth. In *Proceedings of the IEEE/CVF Conference on Computer Vision and Pattern Recognition*, pages 13243–13252, 2022.
- [37] Yu Sun, Qian Bao, Wu Liu, Tao Mei, and Michael J Black. Trace: 5d temporal regression of avatars with dynamic cameras in 3d environments. In *Proceedings of the IEEE/CVF Conference on Computer Vision and Pattern Recognition*, pages 8856–8866, 2023. 2
- [38] Jiayang Tang, Zhaoxi Chen, Xiaokang Chen, Tengfei Wang, Gang Zeng, and Ziwei Liu. Lgm: Large multi-view gaussian model for high-resolution 3d content creation. In *European Conference on Computer Vision*, pages 1–18. Springer, 2024. 2
- [39] Junying Wang, Jae Shin Yoon, Tuanfeng Y Wang, Krishna Kumar Singh, and Ulrich Neumann. Complete 3d human reconstruction from a single incomplete image. In *Proceedings of the IEEE/CVF Conference on Computer vision and Pattern Recognition*, pages 8748–8758, 2023. 3
- [40] Yufu Wang, Yu Sun, Priyanka Patel, Kostas Daniilidis, Michael J Black, and Muhammed Kocabas. Promptmr: Promptable human mesh recovery. In *Proceedings of the Computer Vision and Pattern Recognition Conference*, pages 1148–1159, 2025. 2, 4
- [41] Frederik Warburg, Ethan Weber, Matthew Tancik, Aleksander Holynski, and Angjoo Kanazawa. Nerfbusters: Removing ghostly artifacts from casually captured nerfs. In *Proceedings of the IEEE/CVF International Conference on Computer Vision*, pages 18120–18130, 2023. 3
- [42] Jiaxin Wei, Stefan Leutenegger, and Simon Schaefer. Gsfix3d: Diffusion-guided repair of novel views in gaussian splatting. *arXiv preprint arXiv:2508.14717*, 2025. 2, 3
- [43] Hao Wen, Jing Huang, Huili Cui, Haozhe Lin, Yu-Kun Lai, Lu Fang, and Kun Li. Crowd3d: Towards hundreds of people reconstruction from a single image. In *Proceedings of the IEEE/CVF Conference on Computer Vision and Pattern Recognition*, pages 8937–8946, 2023. 2
- [44] Zhenzhen Weng, Jingyuan Liu, Hao Tan, Zhan Xu, Yang Zhou, Serena Yeung-Levy, and Jimei Yang. Template-free single-view 3d human digitalization with diffusion-guided lrm. *arXiv preprint arXiv:2401.12175*, 2024. 2
- [45] Jay Zhangjie Wu, Yuxuan Zhang, Haithem Turki, Xuanchi Ren, Jun Gao, Mike Zheng Shou, Sanja Fidler, Zan Gojic, and Huan Ling. Difx3d+: Improving 3d reconstructions with single-step diffusion models. In *Proceedings of the Computer Vision and Pattern Recognition Conference*, pages 26024–26035, 2025. 2, 3, 5
- [46] Rundi Wu, Ben Mildenhall, Philipp Henzler, Keunhong Park, Ruiqi Gao, Daniel Watson, Pratul P Srinivasan, Dor Verbin, Jonathan T Barron, Ben Poole, et al. Reconfusion: 3d reconstruction with diffusion priors. In *Proceedings of the IEEE/CVF Conference on Computer Vision and Pattern Recognition*, pages 21551–21561, 2024. 3
- [47] Sibowu, Congrong Xu, Binbin Huang, Andreas Geiger, and Anpei Chen. Genfusion: Closing the loop between reconstruction and generation via videos. In *Proceedings of the Computer Vision and Pattern Recognition Conference*, pages 6078–6088, 2025. 2, 3
- [48] Yichen Xie, Chenfeng Xu, Marie-Julie Rakotosaona, Patrick Rim, Federico Tombari, Kurt Keutzer, Masayoshi Tomizuka, and Wei Zhan. Sparsefusion: Fusing multi-modal sparse representations for multi-sensor 3d object detection. In *Proceedings of the IEEE/CVF International Conference on Computer Vision*, pages 17591–17602, 2023. 3
- [49] Xingyilang Yin, Qi Zhang, Jiahao Chang, Ying Feng, Qingnan Fan, Xi Yang, Chi-Man Pun, Huaqi Zhang, and Xiaodong Cun. Gsfixer: Improving 3d gaussian splatting with reference-guided video diffusion priors. *arXiv preprint arXiv:2508.09667*, 2025. 2, 3
- [50] Hongwen Zhang, Yating Tian, Xinchu Zhou, Wanli Ouyang, Yebin Liu, Limin Wang, and Zhenan Sun. Pymaf: 3d human

- pose and shape regression with pyramidal mesh alignment feedback loop. In *Proceedings of the IEEE/CVF International Conference on Computer Vision*, pages 11446–11456, 2021. [2](#)
- [51] Weitian Zhang, Yichao Yan, Yunhui Liu, Xingdong Sheng, and Xiaokang Yang. E3gen: Efficient, expressive and editable avatars generation. In *Proceedings of the 32nd ACM International Conference on Multimedia*, pages 6860–6869, 2024. [2](#), [3](#)
- [52] Zechuan Zhang, Zongxin Yang, and Yi Yang. Sifu: Side-view conditioned implicit function for real-world usable clothed human reconstruction. In *Proceedings of the IEEE/CVF Conference on Computer Vision and Pattern Recognition*, pages 9936–9947, 2024. [2](#)
- [53] Zerong Zheng, Tao Yu, Yixuan Wei, Qionghai Dai, and Yebin Liu. Deephuman: 3d human reconstruction from a single image. In *Proceedings of the IEEE/CVF International Conference on Computer Vision*, pages 7739–7749, 2019. [5](#), [6](#), [2](#), [4](#)
- [54] Zerong Zheng, Tao Yu, Yebin Liu, and Qionghai Dai. Pamir: Parametric model-conditioned implicit representation for image-based human reconstruction. *IEEE Transactions on Pattern Analysis and Machine Intelligence*, 44(6): 3170–3184, 2021. [2](#)
- [55] Qiang Zhou, Shiyin Wang, Yitong Wang, Zilong Huang, and Xinggang Wang. Human de-occlusion: Invisible perception and recovery for humans. In *Proceedings of the IEEE/CVF Conference on Computer Vision and Pattern Recognition*, pages 3691–3701, 2021. [2](#)
- [56] Shengkun Zhu, Chengcheng Guo, Yuanji Lu, Zhehao Shen, Yize Wu, Yu Hong, Yiwen Cai, Meihan Zheng, Yingliang Zhang, Lan Xu, and Jingyi Yu. A general framework for gaussian splatting-based human-centric volumetric videos. *Visual Intelligence*, 4(8), 2026. [3](#)
- [57] Zehao Zhu, Zhiwen Fan, Yifan Jiang, and Zhangyang Wang. Fsgs: Real-time few-shot view synthesis using gaussian splatting. In *European Conference on Computer Vision*, pages 145–163. Springer, 2024. [3](#)
- [58] Yiyu Zhuang, Jiayi Lv, Hao Wen, Qing Shuai, Ailing Zeng, Hao Zhu, Shifeng Chen, Yujiu Yang, Xun Cao, and Wei Liu. Idol: Instant photorealistic 3d human creation from a single image. In *Proceedings of the Computer Vision and Pattern Recognition Conference*, pages 26308–26319, 2025. [2](#), [3](#), [5](#), [6](#), [7](#)

CrowdGaussian: Reconstructing High-Fidelity 3D Gaussians for Human Crowd from a Single Image

Supplementary Material



Figure 9. Visualization of the multi-stage occlusion mask generation process. From left to right: original image, with keypoint-based elliptical occlusions applied, further corrupted by irregular Bézier-based erasures, and finally smoothed via morphological operations.

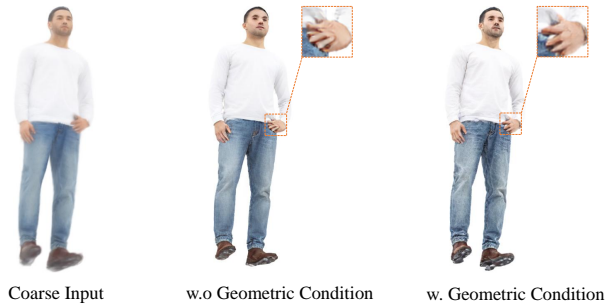


Figure 10. Ablation on geometric conditioning using SMPL normal maps. Left: Coarse input. Middle: Result without normal map conditioning — suffers from hand collapse and facial distortion. Right: Result with normal map — preserves correct hand structure and facial geometry. Zoom-ins show significant improvement in local detail fidelity and structural coherence.

A. Occlusion Simulation for Self-Supervised Training

To ensure robust generalization under real-world occlusions, we design a structured yet diverse masking strategy to synthesize I_{occ} from the full image I_{full} . The occlusion process combines three complementary components: anatomically plausible local erasures, global irregular masks, and structural line cuts—ensuring both realism and diversity in training data.

First, we detect human body keypoints using MediaPipe Pose [24], excluding head landmarks to focus on torso and

limb regions. For each selected keypoint $\mathbf{p}_k = (x_k, y_k)$, we apply an elliptical occlusion:

$$\mathcal{M}_{\text{ellipse}}^{(k)} = \left\{ (x, y) \in \mathbb{R}^2 \mid \frac{(x - x_k)^2}{a_x^2} + \frac{(y - y_k)^2}{a_y^2} \leq 1 \right\}, \quad (7)$$

where semi-axes $a_x, a_y \sim \mathcal{U}(30, 100)$ and rotation angle $\theta \sim \mathcal{U}(0^\circ, 360^\circ)$ are sampled randomly. Up to $K = 5$ such ellipses are applied, with number and location randomized per instance.

Second, we generate large-scale irregular masks using Bézier curves. A quadratic Bézier path is defined by three control points $\mathbf{C}_0, \mathbf{C}_1, \mathbf{C}_2 \in [0, H] \times [0, W]$, uniformly sampled across the image. The curve is thickened into a filled region via polygon rasterization, forming a continuous occluding band:

$$\mathcal{M}_{\text{bezier}} = \bigcup_{i=1}^{N_b} \text{FillPoly}(\text{Bezier}(\mathbf{C}_0^{(i)}, \mathbf{C}_1^{(i)}, \mathbf{C}_2^{(i)}, t), t \in [0, 1]), \quad (8)$$

where $N_b \sim \mathcal{U}\{0, 5\}$ controls the number of such global erasures.

Third, with probability $p = 0.5$, we apply a random straight-line cut that partitions the image into two half-planes. Given two random points $(x_1, y_1), (x_2, y_2)$, the dividing line is:

$$L(x, y) = (y - y_1)(x_2 - x_1) - (x - x_1)(y_2 - y_1) > 0. \quad (9)$$

We select one side for occlusion, ensuring the masked area does not exceed 70% of the total to preserve sufficient visible content.

The final binary mask $\mathcal{M}_{\text{final}}$ is obtained by combining all components:

$$\mathcal{M}_{\text{final}} = \mathcal{M}_{\text{ellipse}} \cup \mathcal{M}_{\text{bezier}} \cup \mathcal{M}_{\text{line}}, \quad (10)$$

followed by morphological closing and dilation (kernel size 5×5 , iterations=3) to smooth boundaries and simulate realistic cloth or object overlap.

As illustrated in Figure 9, this multi-step process progressively constructs complex occlusions that mimic real-world scenarios—such as one person being partially blocked by another or obscured by foreground objects.

This multi-level occlusion scheme ensures that the student model (LORM) learns to recover missing geometry under diverse and challenging conditions, while the frozen teacher provides consistent pseudo-ground truths for stable

self-distillation. During training, we render the 3DGS representation from 24 horizontally distributed camera viewpoints uniformly placed on a full 360-degree orbit around the subject, ensuring comprehensive geometric coverage for robust self-supervised learning.

B. Effect of Geometric Conditioning

To evaluate the impact of geometric priors in diffusion-based refinement, we ablate the use of SMPL normal maps as conditioning input. As shown in Figure 10, without geometric guidance (middle), the refiner often produces structural distortions—such as collapsed hands or misaligned limbs—due to ambiguous depth and pose cues in coarse renderings. In contrast, when conditioned on the SMPL normal map (right), our method preserves anatomically plausible hand and facial structures, demonstrating improved 3D consistency.

The zoom-in views highlight that geometric conditioning helps recover fine-scale details that are otherwise hallucinated or distorted. This confirms that the normal map provides effective 3D-aware inductive bias, guiding the diffusion process to respect human body geometry during refinement.

C. Limitations of 2D Inpainting as Preprocessing

A natural alternative to our self-supervised adaptation framework is to first apply 2D image inpainting to occluded person crops and then feed the completed image into a pre-trained 3D generator such as LHM [29]. However, we find this strategy ineffective due to the inherent limitations of 2D inpainting under real-world occlusions.

As shown in Figure 13, while modern diffusion-based inpainters [1] can generate visually plausible textures locally, they often produce boundary artifacts, inconsistent lighting, and semantically implausible content—such as incorrect limb structures or mismatched clothing patterns. These errors are not only visually jarring but also mislead the downstream 3D reconstruction model.

When such inpainted images are passed to LHM, the generated 3DGS exhibits amplified artifacts, including distorted geometry and texture inconsistencies across views. This confirms that 2D inpainting lacks 3D-awareness and cannot reliably recover structurally coherent human shapes under arbitrary occlusion patterns.

D. More Results

We present additional qualitative results to further demonstrate the effectiveness and generalization of our method.

Figure 11 compares our method against recent state-of-the-art approaches—including LHM [29], PSHuman [18],

SyncHuman [5], and IDOL [58]—on occluded reconstructions from THuman2.1 [53]. The occlusions are synthesized using either Bézier curves or random rectangular masks.

Figure 12 shows reconstructions on a variety of challenging in-the-wild images containing multiple individuals.

E. Multi-Person Human Mesh Recovery

This section provides background on parametric human modeling and multi-person 3D human recovery from a single image, which forms the foundation of our pipeline.

Human Parametric Model The SMPL [23] and SMPL-X parametric model [23, 26] are widely used for representing 3D human body shape and pose. It represents a deformable human mesh as a function of low-dimensional parameters:

$$\mathcal{M}(\beta, \theta) = \mathcal{W}(\mathcal{V}(\beta, \theta), \mathcal{J}(\beta), \mathcal{T}_p(\theta), \mathcal{W}), \quad (11)$$

where $\beta \in \mathbb{R}^{10}$ denotes the shape parameters (learned from PCA over 3D scans), and $\theta \in \mathbb{R}^{23 \times 3}$ represents the joint rotation angles in axis-angle form. The model applies linear blend skinning (\mathcal{W}) to a template mesh \mathcal{V} , with pose-dependent blend shapes and joint regressor $\mathcal{J}(\beta)$ to generate realistic articulations.

Multi-Person Human Mesh Recovery from a Single Image

To recover multiple humans from a single image, recent methods [4, 40] estimate per-person SMPL-X parameters along with their camera-space positions. Given an input image I , the goal is to infer a set of parameters for each detected individual $i = 1, \dots, N$:

$$\{\theta_i, \beta_i, \mathbf{t}_i\}_{i=1}^N = f_{\text{pose}}(I), \quad (12)$$

where θ_i and β_i are the pose and shape parameters of person i , and $\mathbf{t}_i \in \mathbb{R}^3$ is the root translation (camera-relative position).

In our pipeline, we adopt PromptHMR [40] to extract these parameters, which provides robust multi-person pose and global positioning, serving as input for subsequent processing stages.

F. Implementation Details

LORM Training. For efficient fine-tuning, we update the transformer block using LoRA with rank 32, while other inherited pre-trained components remain frozen. The model is trained for approximately 2,000 iterations using the AdamW [15] optimizer with a learning rate of 1×10^{-4} .

CrowdRefiner Training. We build CrowdRefiner based on SD-Turbo [32], employing a single-step diffusion process with noise level $\tau = 200$ (maximum diffusion time

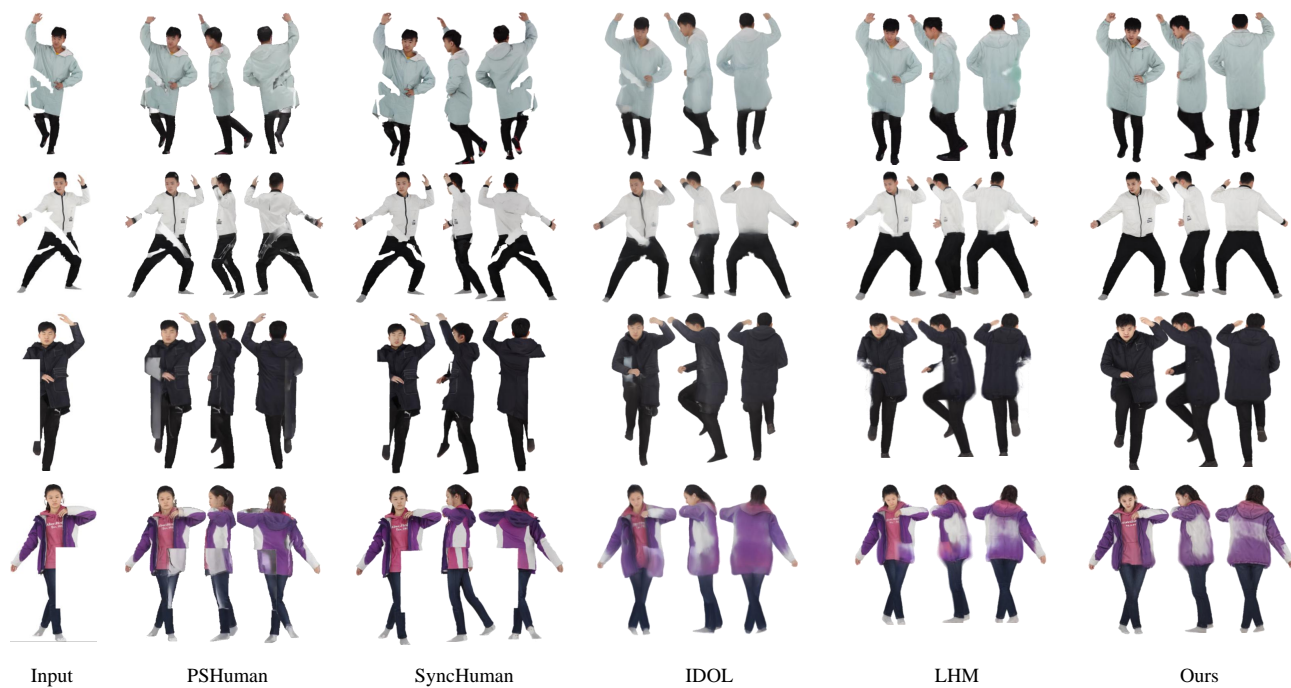


Figure 11. Qualitative comparison on occluded human reconstruction (THuman2.1). Input images are occluded via Bézier curves or rectangular masks.



Figure 12. More reconstruction results on diverse in-the-wild multi-person images.

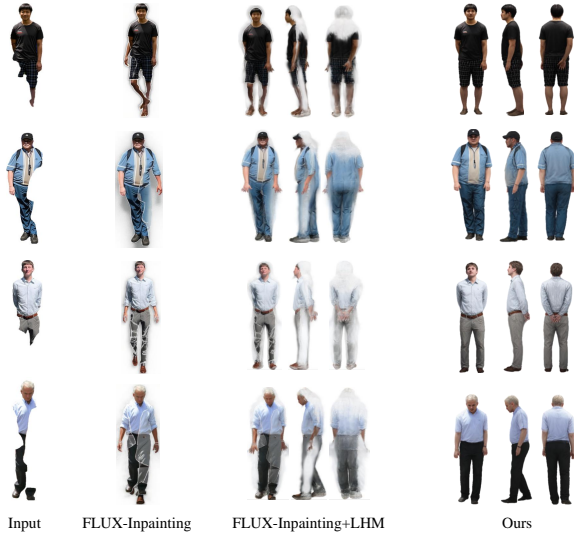


Figure 13. Comparison with the 2D inpainting + LHM pipeline.

$\tau = 1000$), enabling efficient training and inference. We apply LoRA to the VAE decoder with rank 4, while keeping the encoder frozen. The model is trained with the composite loss $\mathcal{L}_{\text{diffuse}}$ for approximately 10,000 steps with a batch size of 2. We apply the SCL strategy by replacing the input with R_{gt} at probability $\rho = 0.2$ during training. The model is optimized using AdamW [15] with a learning rate of 2×10^{-5} .

Evaluation Setup on THuman2.1 For quantitative evaluation on occluded human reconstruction, we select 500 samples from THuman2.1 [53]. Ground truth renderings are generated by rendering the high-fidelity meshes from 24 uniformly distributed viewpoints along a full 360-degree horizontal orbit. These views serve as reference images for computing PSNR, SSIM, and LPIPS to assess reconstruction quality.

G. Evaluation Metrics

We evaluate the performance of CrowdRefiner and compare our method with baselines on occluded human reconstruction using three widely adopted image quality metrics: PSNR, SSIM, and LPIPS. These provide complementary insights into reconstruction fidelity—from pixel accuracy to perceptual similarity.

PSNR Peak Signal-to-Noise Ratio (PSNR) measures the pixel-wise similarity between the predicted rendering I_{pred} and the ground truth I_{gt} . It is computed based on the mean squared error (MSE):

$$\text{MSE} = \frac{1}{N} \sum_p (I_{\text{pred}}[p] - I_{\text{gt}}[p])^2, \quad (13)$$

where p indexes all pixels. The PSNR is then:

$$\text{PSNR} = 10 \cdot \log_{10} \left(\frac{\text{MAX}^2}{\text{MSE}} \right), \quad (14)$$

with MAX as the maximum pixel value (e.g., 255). Higher values indicate better photometric accuracy.

SSIM Structural Similarity (SSIM) evaluates how well structural patterns—such as edges and textures—are preserved. Instead of global statistics, it computes similarity in local windows using luminance, contrast, and structure comparisons:

$$\text{SSIM}(I_{\text{pred}}, I_{\text{gt}}) = \frac{(2\mu_p\mu_g + C_1)(2\sigma_{pg} + C_2)}{(\mu_p^2 + \mu_g^2 + C_1)(\sigma_p^2 + \sigma_g^2 + C_2)}, \quad (15)$$

where μ, σ denote local means and standard deviations, and σ_{pg} is the cross-covariance. Constants C_1, C_2 prevent division by zero. The final score is averaged over all patches. Values closer to 1 indicate stronger structural consistency.

LPIPS Learned Perceptual Image Patch Similarity (LPIPS) assesses perceptual quality by comparing deep features from a pre-trained network. Rather than raw pixels, it operates in feature space:

$$\text{LPIPS}(I_{\text{pred}}, I_{\text{gt}}) = \sum_l w_l \cdot \|\phi_l(I_{\text{pred}}) - \phi_l(I_{\text{gt}})\|_2^2, \quad (16)$$

where ϕ_l extracts features from layer l of a VGG-16 [34] backbone, and w_l are learned weights that emphasize semantically meaningful layers. Lower LPIPS values correspond to higher perceptual similarity, aligning closely with human judgment.

Together, these metrics allow us to assess reconstructions from multiple perspectives: PSNR for pixel-level accuracy, SSIM for structural coherence, and LPIPS for high-level visual realism.

H. Source of In-the-Wild Images

The in-the-wild multi-person images used in our qualitative evaluation are collected from publicly available sources on the web, including search engines such as Google Images [2]. These images are selected solely for visual demonstration and are not used in quantitative benchmarking. We ensure that all displayed examples fall under fair use for academic illustration, with no commercial intent. For reproducibility, we do not claim ownership of these images and encourage readers to refer to the original sources via the search engine.